nature physics

LETTERS

PUBLISHED ONLINE: 28 SEPTEMBER 2015 | DOI: 10.1038/NPHYS3485

Gate-tunable topological valley transport in bilayer graphene

Mengqiao Sui[1,2], Guorui Chen[1,2], Liguo Ma[1,2], Wen-Yu Shan[3], Dai Tian[1,2], Kenji Watanabe[4], Takashi Taniguchi[4], Xiaofeng Jin[1,2], Wang Yao[5], Di Xiao[3] and Yuanbo Zhang[1,2]*

Valley pseudospin, the quantum degree of freedom characterizing the degenerate valleys in energy bands[1], is a distinct feature of two-dimensional Dirac materials[1–5]. Similar to spin, the valley pseudospin is spanned by a time-reversal pair of states, although the two valley pseudospin states transform to each other under spatial inversion. The breaking of inversion symmetry induces various valley-contrasted physical properties; for instance, valley-dependent topological transport is of both scientific and technological interest[2–5]. Bilayer graphene is a unique system whose intrinsic inversion symmetry can be controllably broken by a perpendicular electric field, offering a rare possibility for continuously tunable topological valley transport. We used a perpendicular gate electric field to break the inversion symmetry in bilayer graphene, and a giant nonlocal response was observed as a result of the topological transport of the valley pseudospin. We further showed that the valley transport is fully tunable by external gates, and that the nonlocal signal persists up to room temperature and over long distances. These observations challenge the current understanding of topological valley transport in a gapped system, and the robust topological transport may lead to future valleytronic applications.

In crystalline solids, a topological current can be induced by the Berry phase of the electronic wavefunction[6]. Examples include the quantum Hall current in a magnetic field, and the spin Hall current arising from spin–orbit coupling[7]. Such topological transport is robust against impurities and defects in materials—a feature that is much sought after in potential electronic applications. In such applications, the ability to switch and to continuously tune the topological transport is crucial. The topological current is in principle dictated by the crystal symmetry, which is difficult to change in bulk materials. Bilayer graphene (BLG), however, offers new opportunities in which inversion symmetry can be controllably broken by an external electric field in the perpendicular direction.

The topological current controlled by the inversion symmetry breaking is associated with carriers' valley pseudospin, which characterizes the twofold degenerate band edges located at the corners of the hexagonal Brillouin zone. The topological Hall current, odd under time reversal but even under inversion, is strictly zero in pristine mono- and bilayer graphene, which respect both symmetries. When the inversion symmetry is broken, however, time-reversal symmetry requires the Hall currents to have opposite signs and equal magnitudes in the two valleys (that is, a valley Hall effect), as recently demonstrated in monolayer graphene[4]. Microscopically, inversion symmetry breaking opens a bandgap at the charge neutral point (CNP), and produces valley-contrasted Berry curvatures[2]. The Berry curvatures act similarly to a momentum-space magnetic field that causes the Hall effect at finite doping[6]. In BLG, the inversion symmetry (and the Berry curvature) is for the first time controlled by gate electric field. Valley Hall current is therefore expected to be fully tunable by external gates, bringing topological transport in line with modern electronic technology.

In this study, we demonstrated tunable topological valley Hall transport in gate-biased BLG with nonlocal measurement in a Hall bar configuration (Fig. 1a and c inset), which has been used to detect nonlocal transport in other spin/pseudospin systems[4,8–11]. The charge current injected at one end of the Hall bar induced a pure valley Hall current in the transverse direction and, because of the inverse valley Hall effect, converted to a charge imbalance at the other end of the sample; we therefore detected a nonlocal response as a voltage drop. We demonstrated that the giant, tunable, nonlocal response can be induced by the perpendicular gate electric field, but is absent in the gapless BLG in which inversion symmetry is present. Such gate tunability indicates the essential role of inversion symmetry breaking in nonlocal transport, and provides unambiguous evidence that our nonlocal signal was a result of the valley Hall effect. The nonlocal transport persists up to room temperature and over long distances (up to 10 μm). Our results represent major progress in the quest for a robust, tunable valley pseudospin system among various alternatives[3–5,12,13], and indicate the possibility of using the nonlocal topological transport in practical applications under ambient conditions.

The structure of our dual-gate graphene field-effect transistors (FETs) is shown in Fig. 1a,b. We constructed the device by sequentially transferring BLG and hexagonal boron nitride (hBN) flakes onto an hBN substrate supported on a SiO_2/Si wafer (SiO_2 thickness = 300 nm). Before the deposition of the top hBN flake, BLG was etched into a well-defined Hall bar geometry (Fig. 1a, broken line) for easy characterization in both local and nonlocal configurations. The whole stack was etched again after the deposition of the top hBN to expose the graphene edge for making electrical contacts with metallic leads[14] (Cr/Au, 8 nm and 70 nm, respectively). The final device had BLG sandwiched between the top and bottom gates (Fig. 1b), and the hBN gate dielectric ensured excellent sample quality (see Methods).

Voltages applied on top and bottom gates (V_t and V_b) enabled us to independently control the gap opening and carrier doping in the BLG. The bandgap E_g is determined by the average of top- and bottom-gate-induced electrical displacement fields,

[1]State Key Laboratory of Surface Physics and Department of Physics, Fudan University, Shanghai 200433, China. [2]Collaborative Innovation Center of Advanced Microstructures, Shanghai 200433, China. [3]Department of Physics, Carnegie Mellon University, Pittsburgh, Pennsylvania 15213, USA. [4]Advanced Materials Laboratory, National Institute for Materials Science, 1-1 Namiki, Tsukuba, 305-0044, Japan. [5]Department of Physics and Center of Theoretical and Computational Physics, University of Hong Kong, Hong Kong, China. *e-mail: zhyb@fudan.edu.cn

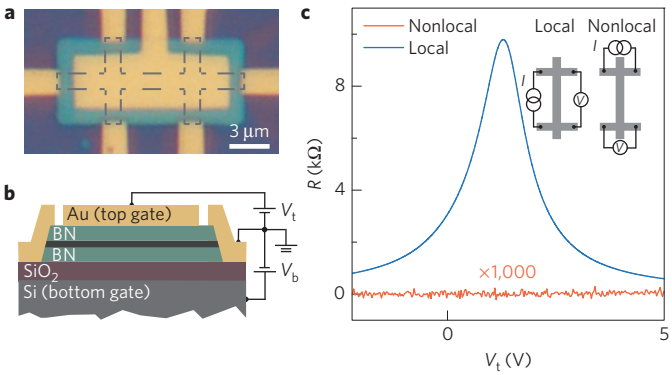

Figure 1 | Dual-gated BLG FET and its local and nonlocal characterization. **a**, Optical image of a typical BLG FET viewed from the top. A BLG Hall bar (outlined by a broken line) is sandwiched between the top and bottom hBN flakes. The hBN/BLG/hBN stack (blue) was etched to expose the BLG leads at the edge that are subsequently contacted by Au electrodes (orange). **b**, Schematic cross-sectional view of the device shown in **a**. An Au pad and degenerately doped silicon served as top and bottom gates, respectively. **c**, Local and nonlocal resistance measured as a function of top-gate voltage V_t while the bottom-gate voltage V_b was fixed at −7.5 V. BLG should have a zero bandgap at the CNP (see Fig. 2e), and nonlocal signal was not detected under this condition. Inset: illustration of the local and nonlocal measurement set-up.

$D=(D_t+D_b)/2$, which breaks the inversion symmetry of the BLG (ref. 15). The carrier doping n can be tuned by the difference of the two displacement fields, $n=\varepsilon_0(D_t-D_b)$, where ε_0 is the vacuum permittivity. In our experiment, the drain electrode was grounded, and the displacement fields were related to top- and bottom-gate voltages by $D_t=-\varepsilon_t(V_t-V_{t0})/d_t$ and $D_b=\varepsilon_b(V_b-V_{b0})/d_b$, where ε and d are the dielectric constant and thickness of the dielectric layers, respectively, and V_{t0} and V_{b0} are effective offset voltages caused by environment-induced carrier doping. The resistance of our sample measured in a standard four-terminal set-up (referred to as local resistance R_L) exhibited the typical behaviour of BLG: the CNP manifested as a peak in R_L as the carrier density was varied in a pristine sample (Fig. 1c, blue), and the peak value increased substantially as a bandgap was opened by a finite field D (Fig. 2a–d, blue). R_L plotted as a function of both V_t and V_b shows the effect of gate bias more clearly in Fig. 2e. Along the line defined by the (V_t, V_b) pairs at the CNP, the bandgap is fully tuned by D, whereas the sample remained charge neutral. The sample exhibited a net charge doping perpendicular to the line in the (V_t, V_b) plane, with the bandgap remaining constant.

A pronounced nonlocal response appeared as the bandgap opened in BLG at low temperatures. We detected the response by sending a current I through the local leads, and sensing the nonlocal voltage V_{NL} at the far end of the sample (see Fig. 1c inset for the measurement set-up). The nonlocal resistance R_{NL}, defined as $R_{NL}=V_{NL}/I$, is negligible in a pristine sample with zero gap opening (Fig. 1c, orange). A peak in R_{NL}, however, appeared at a threshold displacement field of $D=0.28\,\mathrm{V\,nm^{-1}}$, and increased rapidly to the order of a few hundred Ω at large D (Fig. 2a–d, data obtained at temperature $T=70\,\mathrm{K}$). The two-dimensional plot of R_{NL} as a function of V_t and V_b shows the general behaviour of the nonlocal response at $T=70\,\mathrm{K}$ (Fig. 2f). R_{NL} generally peaks at the CNP, but two features distinguish the behaviour of R_{NL} from that of the local resistance R_L: the R_{NL} peak is generally sharper than the R_L peak, and R_{NL} drops to zero outside the peak whereas R_L maintains an order of approximately 100 kΩ at finite doping. Both features indicate the distinct origins of R_{NL} and R_L, and are general behaviour of nonlocal transport observed in other graphene pseudospin and spin systems[4,8,10]. In the present study, we noted that the peak positions of R_{NL} and R_L were not always aligned with each other; we attribute the misalignment to inhomogeneities that were present in our samples (Supplementary Section IV). We emphasize that the observed R_{NL} was not from the stray charge current that contributes an ohmic nonlocal resistance[8]. Such ohmic contribution decreases exponentially with the sample length-to-width ratio L/w, and is up to two orders of magnitude lower than the observed R_{NL} in the device shown in Fig. 2a–d ($L=5\,\mu\mathrm{m}$ and $w=1.5\,\mu\mathrm{m}$; the ohmic contribution to R_{NL} is represented by the broken line). A pronounced nonlocal signal was observed in devices with an even higher L/w ratio of up to 6.7 (Fig. 3e).

The temperature dependence of R_{NL} and R_L revealed crucial information on the microscopic mechanism of both the local and nonlocal transport. Three distinct transport regimes were observed at large fields (Fig. 3a): thermal activation at high temperature; nearest-neighbour hopping at intermediate temperature; and variable-range hopping at low temperature. These transport regimes were consistent with previous studies[16,17] (Supplementary Section V). In particular, the high-temperature activation behaviour enabled us to extract the BLG bandgap E_g as a function of D, which agreed well with theoretical calculations and previous measurements[15,16] (Fig. 3a inset and Supplementary Section V).

Pronounced nonlocal signal is observed in both thermal activation and hopping regimes (Fig. 3b). We found that R_{NL} also followed an exponential activated behaviour in the thermal activation regime at high temperatures (Fig. 3b inset), although with an exponent higher than $E_g/2k_BT$ (Supplementary Fig. 5d). The connection between R_{NL} and R_L became obvious when $\ln R_{NL}$ was plotted against $\ln R_L$ (Fig. 3c). Data sets for different D were all in straight lines with the same slope $\alpha=2.77\pm0.02$ in the thermal activation regime; hence, a simple relation $R_{NL}\sim R_L^{\alpha}$ can be established. We noted that a diffusive nonlocal topological transport model indeed predicted a power-law relation $R_{NL}\sim R_L^3\sigma_{xy}^2\,\mathrm{e}^{-L/\lambda_v}/\lambda_v$ (ref. 18), where σ_{xy} is the valley Hall conductivity, and λ_v is the valley diffusion length. Our observation agreed reasonably well with this predicted scaling between R_{NL} and R_L, and the deviation of α from 3 may indicate the complicated role of σ_{xy} and/or λ_v in R_{NL}. α varied among samples, probably as a result of differences in sample disorder (Supplementary Fig. 6). Intriguingly, our data show that the simple relation $R_{NL}\sim R_L^{\alpha}$ persists beyond the thermal activation regime and into the hopping regime until the curves eventually level off (Fig. 3c). The same power law also describes the scaling relation between R_{NL} and R_L (with an α close to 3) at finite carrier densities (Supplementary Section X).

The widely tunable bandgap in BLG provides another crucial benefit, which is the room-temperature operation of our BLG nonlocal FET. Figure 3d shows the R_{NL} observed up to room temperature in a BLG biased at $D=-1.23\,\mathrm{V\,nm^{-1}}$ (corresponding to $E_g=135\,\mathrm{meV}$). A wide bandgap alone does not guarantee high-temperature nonlocal transport because the nonlocal signal, along with R_L, decreases exponentially with temperature in the thermal activation regime. However, R_{NL} does not decrease as rapidly with increasing temperature in the hopping regime. When the onset of the hopping regime occurs at high temperatures, room-temperature operation consequently remains possible. The key, therefore, is to find samples in which the onset of the hopping regime occurs at near room temperature, as we have demonstrated in the samples shown in Fig. 3d and Supplementary Fig. 7.

We now turn to the length dependence of the nonlocal valley transport. Here we note the analogy between the valley transport in biased BLG and the spin transport in which spin-flip scattering causes the spin diffusion current to decay exponentially. The valley

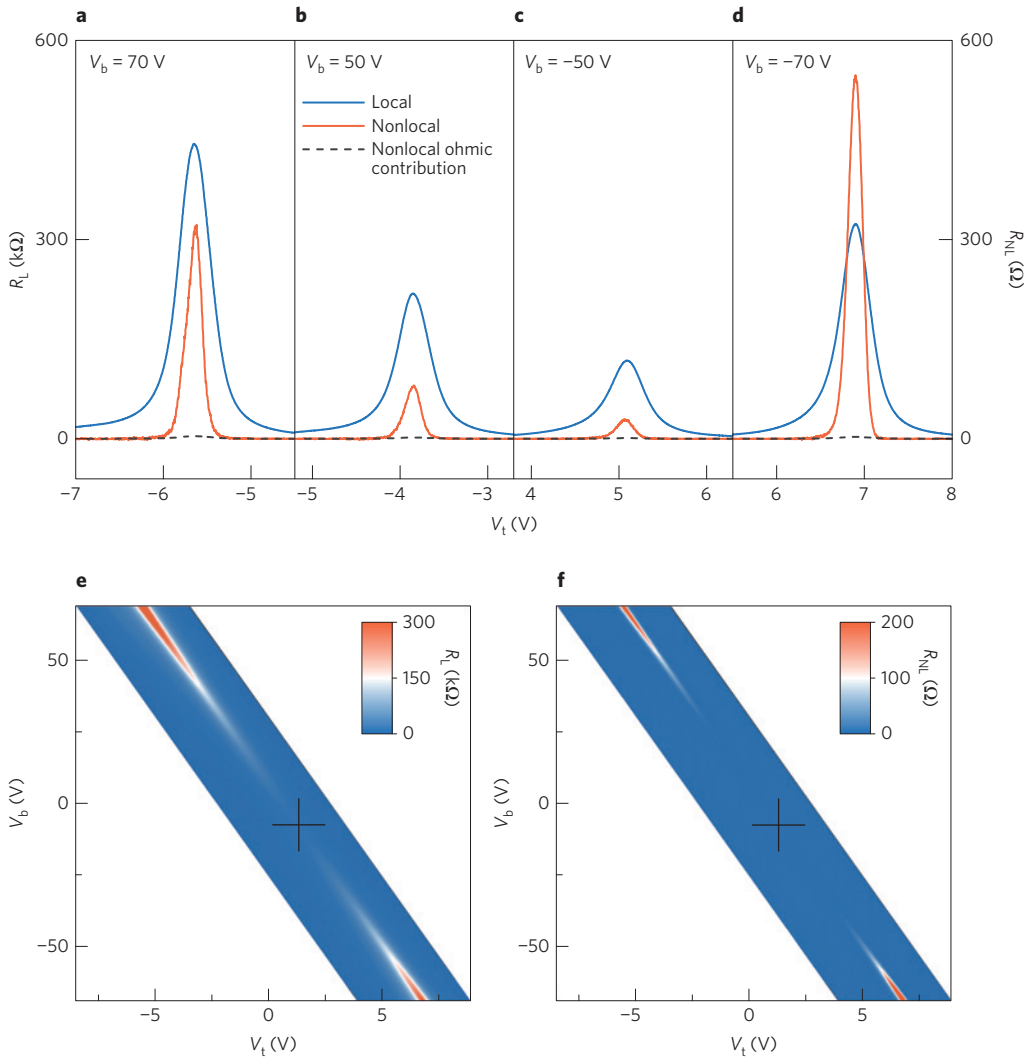

Figure 2 | Local and nonlocal response of biased BLG. a–d, Local and nonlocal resistance as a function of V_t with V_b fixed at varying voltages. The length and width of the sample were 5 μm and 1.5 μm, respectively. The dashed lines show the expected ohmic nonlocal contribution (see text), which is substantially smaller than the actual measured R_{NL} (orange curves). **e**,**f**, Local and nonlocal resistance measured as a function of both V_t and V_b. Data were obtained from the same device measured in **a–d** and Fig. 1c. The crosses mark the point $(V_{t0}, V_{b0}) = (1.3\,V, -7.5\,V)$ where no bandgap opened in BLG. All data were recorded at $T = 70$ K.

current in BLG decreases through intervalley scattering, which requires a large momentum transfer (for example, by atomic-scale disorders). Such disorders are found to be extremely rare in cleaved BLG crystals[19,20], implying a large valley diffusion length λ_v (refs 21,22). In the present study, an appreciable nonlocal signal was observed in samples up to 10 μm long. Figure 3e shows the length-dependent R_{NL}, measured on a single device under a field of $D = -0.47\,V\,nm^{-1}$. From a line fit to the semilog plot of the R_{NL} peak value as a function of sample length (Fig. 3e inset), we obtained an order of magnitude estimation $\lambda_v \sim 1$ μm, and sample inhomogeneity (manifested as a shift of R_{NL} peaks in Fig. 3e) prevents a more precise estimation. Such a large length scale agrees reasonably well with recent studies on intervalley scattering[21,22], and is also consistent with the areal density of atomic defects ($12.05\,\mu m^{-2}$) found in Kish graphite[23], which is the same type of specimen used in this study.

The observation of a giant nonlocal response in the middle of the energy gap in insulating BLG was unexpected. Although midgap helical edge states in 2D quantum spin Hall systems can support long-range nonlocal conduction[24–26], such spin helical edge states did not exist in our study because BLG is topologically trivial. Midgap valley helical modes may still exist at topological domain walls or edges of BLG in certain circumstances[27–29], and may potentially lead to nonlocal conduction. The nonlocal transport through edge states and bulk states, however, exhibit markedly different length dependences; for a given sample width, bulk conduction depends on the active length of the sample, whereas the edge state conduction depends only on the length of the edge[8]. We took advantage of this difference to fabricate the device shown in Fig. 4 inset: two Hall bars (left and right with shared current injection leads 2 and 5) have the same active sample length but substantially different edge lengths. The fact that a comparable nonlocal response was observed on both Hall bars unambiguously demonstrates the bulk origin of our valley transport. A robust nonlocal response with the same sign and order of magnitude was observed in all of the samples that we fabricated on hBN (6 in total). Helical modes at the domain walls, which differ according to sample if they exist at all, are unlikely to be the origin of the observed nonlocal transport.

The question then arises as to what physical mechanism leads to the nonlocal valley transport that we observed. The valley Hall effect originally proposed in graphene requires finite doping[2], and

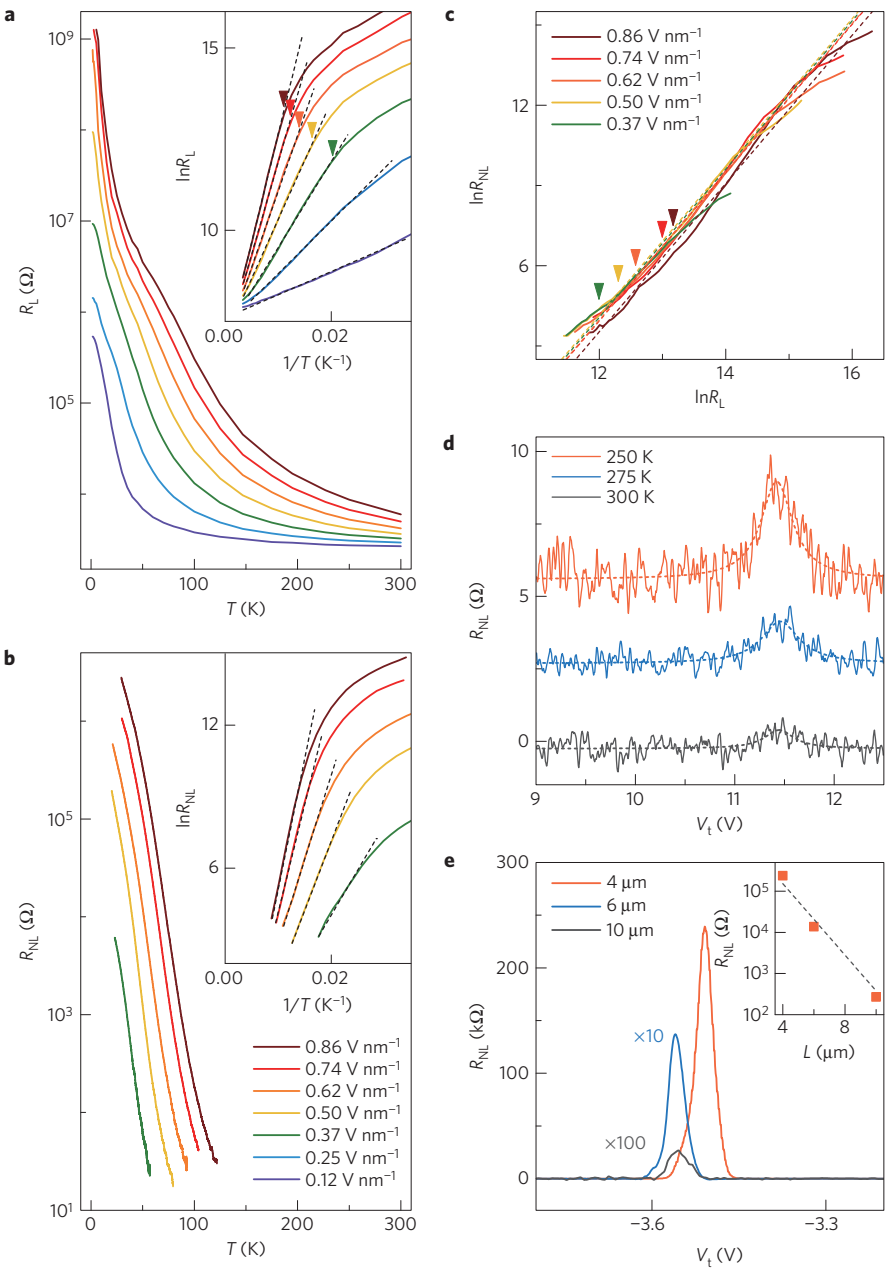

Figure 3 | Temperature and length dependence of the local and nonlocal responses of biased BLG. a, Peak resistance in R_L measured as a function of temperature under varying electric displacement fields. Three transport regimes are clearly visible for displacement field $D > 0.5$ V nm^{-1} (see text). Inset: the Arrhenius plot of R_L showing thermal activation behaviour at high temperatures. Dashed lines are the line fit to the linear part of the Arrhenius plot, and thermal activation energy could be obtained from the slope of the line fit (Supplementary Section V). The triangles mark the onset of the hopping regime. **b**, Peak nonlocal resistance in R_{NL} measured as a function of temperature under varying electric displacement fields. Data were obtained from the same device measured in **a**. Inset: the Arrhenius plot of R_{NL}. R_{NL} also shows thermal activation behaviour at high temperatures, and dashed lines are the line fit. **c**, lnR_L plotted against lnR_{NL} for varying displacement field D. R_{NL} and R_L are from the data sets in **a** and **b**. Triangles mark the onset of the hopping regime shown in **a**. lnR_L scales linearly with lnR_{NL} with a single slope $\alpha = 2.77 \pm 0.02$ for different D in both thermal activation and hopping regimes, before levelling off deep in the hopping regime. The dashed lines are the line fit to the linear part of the data sets. **d**, High-temperature R_{NL} obtained in a sample in which the onset of the hopping regime occurred at near room temperature (see text). The curves are shifted for clarity. The dashed lines are a visual guide. The bottom gate was fixed at $V_b = -100$ V. **e**, Length dependence of nonlocal response. Hall bars with different length L were fabricated on a single a device. R_{NL} was measured at different L with $V_b = 30$ V and $T = 20$ K. Sample width: 1.5 μm. Inset: semilog plot of peak values of R_{NL} as a function of L. The dashed line is a visual guide that corresponds to a valley diffusion length of approximately 1 μm.

is therefore not applicable in our insulating BLG. To this end, we note that nonlocal valley transport in an insulator without helical edge states is an area still open to theoretical investigation[30], and theories on the anomalous Hall effect in insulating ferromagnetic materials may provide important clues[31–33]. Our results call for a continued effort, both experimental and theoretical, to address this outstanding problem.

Note added in proof: We became aware of a related work on the topological valley transport in gated bilayer graphene[34].

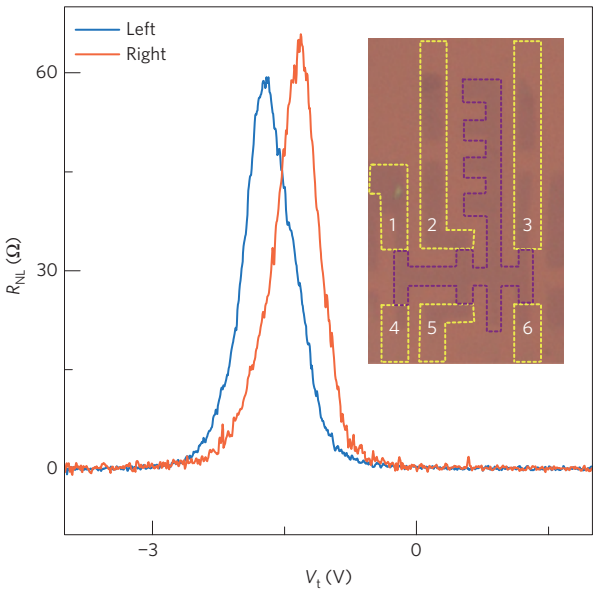

Figure 4 | Bulk versus edge nonlocal transport. Nonlocal resistance as a function of V_t (V_b fixed at 50 V) obtained on two Hall bars (left and right) shown in the inset. Data were obtained at $T = 30$ K. The two Hall bars share two local leads (contact 2 and 5) in the middle, and the left and right Hall bars have the same active sample length but substantially different edge lengths. We passed current through the two local leads and measured R_{NL} at the far end of the left Hall bar (contact 1 and 4) and right Hall bar (contact 3 and 6). Nonlocal signal was detected with similar amplitude on both the left and right Hall bars, indicating the bulk origin of the nonlocal transport. Inset: BLG sample on a hBN substrate before deposition of the top hBN flake. The purple dashed line outlines the geometry of the etched BLG, and the yellow dashed lines indicate the position of the electrodes to be deposited.

Methods

Methods and any associated references are available in the online version of the paper.

Received 24 January 2015; accepted 21 August 2015; published online 28 September 2015

References

1. Xu, X., Yao, W., Xiao, D. & Heinz, T. F. Spin and pseudospins in layered transition metal dichalcogenides. *Nature Phys.* **10,** 343–350 (2014).
2. Xiao, D., Yao, W. & Niu, Q. Valley-contrasting physics in graphene: Magnetic moment and topological transport. *Phys. Rev. Lett.* **99,** 236809 (2007).
3. Mak, K. F., McGill, K. L., Park, J. & McEuen, P. L. The valley Hall effect in MoS_2 transistors. *Science* **344,** 1489–1492 (2014).
4. Gorbachev, R. V. *et al.* Detecting topological currents in graphene superlattices. *Science* **346,** 448–451 (2014).
5. Xiao, D., Liu, G.-B., Feng, W., Xu, X. & Yao, W. Coupled spin and valley physics in monolayers of MoS_2 and other group-VI dichalcogenides. *Phys. Rev. Lett.* **108,** 196802 (2012).
6. Xiao, D., Chang, M.-C. & Niu, Q. Berry phase effects on electronic properties. *Rev. Mod. Phys.* **82,** 1959–2007 (2010).
7. Nagaosa, N., Sinova, J., Onoda, S., MacDonald, A. H. & Ong, N. P. Anomalous Hall effect. *Rev. Mod. Phys.* **82,** 1539–1592 (2010).
8. Abanin, D. A. *et al.* Giant nonlocality near the Dirac point in graphene. *Science* **332,** 328–330 (2011).
9. Hoffmann, A. Spin Hall effects in metals. *IEEE Trans. Magn.* **49,** 5172–5193 (2013).
10. Balakrishnan, J., Kok Wai Koon, G., Jaiswal, M., Castro Neto, A. H. & Özyilmaz, B. Colossal enhancement of spin–orbit coupling in weakly hydrogenated graphene. *Nature Phys.* **9,** 284–287 (2013).
11. Wang, Z., Tang, C., Sachs, R., Barlas, Y. & Shi, J. Proximity-induced ferromagnetism in graphene revealed by the anomalous Hall effect. *Phys. Rev. Lett.* **114,** 016603 (2015).
12. Yao, W., Xiao, D. & Niu, Q. Valley-dependent optoelectronics from inversion symmetry breaking. *Phys. Rev. B* **77,** 235406 (2008).
13. Wu, S. *et al.* Electrical tuning of valley magnetic moment through symmetry control in bilayer MoS_2. *Nature Phys.* **9,** 149–153 (2013).
14. Wang, L. *et al.* One-dimensional electrical contact to a two-dimensional material. *Science* **342,** 614–617 (2013).
15. Zhang, Y. *et al.* Direct observation of a widely tunable bandgap in bilayer graphene. *Nature* **459,** 820–823 (2009).
16. Zou, K. & Zhu, J. Transport in gapped bilayer graphene: The role of potential fluctuations. *Phys. Rev. B* **82,** 081407 (2010).
17. Taychatanapat, T. & Jarillo-Herrero, P. Electronic transport in dual-gated bilayer graphene at large displacement fields. *Phys. Rev. Lett.* **105,** 166601 (2010).
18. Abanin, D. A., Shytov, A. V., Levitov, L. S. & Halperin, B. I. Nonlocal charge transport mediated by spin diffusion in the spin Hall effect regime. *Phys. Rev. B* **79,** 035304 (2009).
19. Decker, R. *et al.* Local electronic properties of graphene on a BN substrate via scanning tunneling microscopy. *Nano Lett.* **11,** 2291–2295 (2011).
20. Xue, J. *et al.* Scanning tunnelling microscopy and spectroscopy of ultra-flat graphene on hexagonal boron nitride. *Nature Mater.* **10,** 282–285 (2011).
21. Engels, S. *et al.* Limitations to carrier mobility and phase-coherent transport in bilayer graphene. *Phys. Rev. Lett.* **113,** 126801 (2014).
22. Couto, N. J. G. *et al.* Random strain fluctuations as dominant disorder source for high-quality on-substrate graphene devices. *Phys. Rev. X* **4,** 041019 (2014).
23. Wu, S., Yang, R., Shi, D. & Zhang, G. Identification of structural defects in graphitic materials by gas-phase anisotropic etching. *Nanoscale* **4,** 2005–2009 (2012).
24. König, M. *et al.* Quantum spin Hall insulator state in HgTe quantum wells. *Science* **318,** 766–770 (2007).
25. Roth, A. *et al.* Nonlocal transport in the quantum spin Hall state. *Science* **325,** 294–297 (2009).
26. Bernevig, B. A., Hughes, T. L. & Zhang, S.-C. Quantum spin Hall effect and topological phase transition in HgTe quantum wells. *Science* **314,** 1757–1761 (2006).
27. Yao, W., Yang, S. A. & Niu, Q. Edge states in graphene: From gapped flat-band to gapless chiral modes. *Phys. Rev. Lett.* **102,** 096801 (2009).
28. Li, J., Martin, I., Büttiker, M. & Morpurgo, A. F. Topological origin of subgap conductance in insulating bilayer graphene. *Nature Phys.* **7,** 38–42 (2011).
29. Alden, J. S. *et al.* Strain solitons and topological defects in bilayer graphene. *Proc. Natl Acad. Sci. USA* **110,** 11256–11260 (2013).
30. Lensky, Y. D., Song, J. C. W., Samutpraphoot, P. & Levitov, L. S. Topological valley currents in gapped Dirac materials. *Phys. Rev. Lett.* **114,** 256601 (2015).
31. Liu, X.-J., Liu, X. & Sinova, J. Scaling of the anomalous Hall effect in the insulating regime. *Phys. Rev. B* **84,** 165304 (2011).
32. Burkov, A. A. & Balents, L. Anomalous Hall effect in ferromagnetic semiconductors in the hopping transport regime. *Phys. Rev. Lett.* **91,** 057202 (2003).
33. Lyanda-Geller, Y. *et al.* Charge transport in manganites: Hopping conduction, the anomalous Hall effect, and universal scaling. *Phys. Rev. B* **63,** 184426 (2001).
34. Shimazaki, Y. *et al.* Generation and detection of pure valley current by electrically induced Berry curvature in bilayer graphene. Preprint at http://arxiv.org/abs/1501.04776 (2015).

Acknowledgements

We thank Q. Niu, D.-H. Lee, F. Wang, J. Shi, J. Xiao, P. Kim and J. Zhu for helpful discussions. Part of the sample fabrication was performed at the Fudan Nano-fabrication Lab. M.S., G.C., L.M. and Y.Z. acknowledge the financial support of the National Basic Research Program of China (973 Program) under grant nos 2013CB921902 and 2011CB921802, and NSF of China under grant nos 11034001 and 11425415. W.Y. acknowledges support from the University of Hong Kong (OYRA), and the RGC of Hong Kong SAR (HKU706412P). W.-Y.S. and D.X. acknowledge support from the US Department of Energy, Office of Science, Office of Basic Energy Science, under award no. DE-SC0012509. D.T. and X.J. are supported by MOST (grants no. 2015CB921400 and no. 2011CB921802) and NSF of China (grants no. 11374057, no. 11434003 and no. 11421404). K.W. and T.T. acknowledge support from the Elemental Strategy Initiative conducted by the MEXT, Japan. T.T. acknowledges support from Grant-in-Aid for Scientific Research (Grant 262480621) and Innovative Areas 'Nano Informatics' (Grant 25106006) from JSPS.

Author contributions

M.S. fabricated the samples, carried out the measurements, and analysed the data. G.C. helped with sample fabrication. L.M. helped with electrical measurements. W.-Y.S. and D.T. helped with data analysis. K.W. and T.T. grew hBN crystals. Y.Z., D.X., W.Y. and X.J. co-supervised the project. All authors contributed to the writing of the manuscript.

Additional information

Supplementary information is available in the online version of the paper. Reprints and permissions information is available online at www.nature.com/reprints. Correspondence and requests for materials should be addressed to Y.Z.

Competing financial interests

The authors declare no competing financial interests.

Methods

Device fabrication. We fabricated BLG devices by following procedures similar to those described previously[14,35]. BLG flakes transferred onto hBN substrate were etched into a Hall bar geometry by using standard electron beam lithography followed by reactive ion etching. The etched BLG Hall bar was then annealed at 370 °C in an Ar/H_2 atmosphere overnight to remove electron beam resist residue. We further cleaned the sample surface by using an atomic force microscope (Park Systems) operating in contact mode[36]. The BLG Hall bar on the hBN substrate was then covered by another layer of hBN as a top-gate dielectric. The hBN/BLG/hBN stack was then etched using inductively coupled plasma to expose graphene leads at the edge. Finally, metal electrodes (Cr/Au, 8 nm and 70 nm) were deposited for electrical contact with graphene leads. The devices exhibited mobility ranging from 1,500 $cm^2\ V^{-1}\ s^{-1}$ to 50,000 $cm^2\ V^{-1}\ s^{-1}$ at 10 K, and nonlocal signal was observed in all of them.

Nonlocal resistance measurement. The high common-mode voltage present in the measurement circuit and the high output impedance of the nonlocal voltage signal cause the typical lock-in measurement to fail at large gate biases when BLG becomes excessively resistive. We found that the problem can be mitigated by increasing the input impedance of the preamplifier of the measurement circuit. Reliable measurement of the nonlocal signal can also be obtained by detecting the current instead of voltage in the nonlocal leads; however, precautions must be taken to float the current preamplifier. A detailed discussion of our nonlocal measurement is presented in Supplementary Section I.

References

35. Taychatanapat, T., Watanabe, K., Taniguchi, T. & Jarillo-Herrero, P. Quantum Hall effect and Landau-level crossing of Dirac fermions in trilayer graphene. *Nature Phys.* **7,** 621–625 (2011).
36. Lindvall, N., Kalabukhov, A. & Yurgens, A. Cleaning graphene using atomic force microscope. *J. Appl. Phys.* **111,** 064904 (2012).